Available online at www.sciencedirect.com
SCIENCE DIRECT®
Journal of Food Engineering 76 (2006) 477–489
JOURNAL OF FOOD ENGINEERING
www.elsevier.com/locate/jfoodeng

Conductive drying kinetics of pregelatinized starch thin films

Thodoris D. Karapantsios *

Department of Chemistry, Division of Chemical Technology, Aristotle University of Thessaloniki, University Box 116, 541 24 Thessaloniki, Greece

Received 19 October 2004; accepted 21 May 2005
Available online 22 July 2005

Abstract

Thin film drying of pregelatinized starch over a hot surface in the absence of forced airflow was investigated by analyzing simultaneous loss-in-weight, heat flow and temperature data records. This kind of drying is chiefly related to drum drying applications. Experiments were performed by varying the film thickness, preparation conditions (pasting temperature and pasting duration) and drying temperature. For the examined range of values, film thickness played the most decisive role in determining the kinetic characteristics of drying. An analysis was conducted testing several heterogeneous reaction kinetic models as well as a semi-empirical model from literature in an effort to identify a suitable rate expression and investigate probable mechanisms of the process. Results indicate that removal of moisture from these thin films follows both a boiling-type and a conductive type of drying. It appears that boiling prevails in the thinner films whereas both mechanisms can exist in the thicker ones.

Keywords: Drum drying; Double-drum dryer; Drying kinetics; Thin film; Conductive drying; Boiling; Starch

1. Introduction

Pregelatinized starches, also referred to as instant starches, are starch/water suspensions that have been simply precooked and drum dried to give products that disperse readily in cold water to form moderately stable suspensions (Hodge & Osman, 1976). Such products are used mainly as thickeners in foods and as adhesives in foundry core binders and in the textile industry (Colonna, Buleo, & Mercier, 1987). Drum drying refers collectively to specific physicochemical modifications of starch granules performed in two stages: gelatinization and drying. Double-drum dryers are especially suitable for this process because of their ability to handle a wider range of products, better economics, more efficient operations, higher production rates and fewer operating labour requirements (Moore, 1995).

In a double-drum dryer, gelatinization takes place inside the "pool" of material formed between the upper halves of two horizontal steam-heated drums, rotating very close together in opposite directions. Although some limited drying occurs already in the pool, the actual drying starts only after the gelatinized material leaves the pool through the narrow gap between the drums and adheres as a thin film on the surface of the drums. This film is no longer in motion relative to the drums because of the rapid drying and solidification. After travelling part of a revolution, the dried film is removed in the form of thin sheets by scraper blades. Thus, drum dryers are conduction dryers, the drying effect being obtained by the transfer of heat from the condensing steam inside the drums to the film of material covering their external surface.

Theoretical modeling of the drum drying process is very important for the design, optimization and control of drum dryers. Yet, it is a very difficult task since drum drying is a really complex process requiring except for a submodel of the drying process itself, a fluid dynamics submodel (for initial film deposition over the drum)

* Tel.: +30 2310 99 77 72; fax: +30 2310 99 77 59.
E-mail address: karapant@chem.auth.gr

0260-8774/$ - see front matter © 2005 Elsevier Ltd. All rights reserved.
doi:10.1016/j.jfoodeng.2005.05.047

and a heat transfer submodel (heat conduction through the drum solid wall). The drying submodel of viscous foodstuffs, has been extensively studied by Vasseur and co-workers (e.g., Abchir, Vasseur, & Trystram, 1988; Daud & Armstrong, 1987, 1988; Trystram, Meot, Vasseur, Abchir, & Couvrat-Desvergnes, 1988; Trystram & Vasseur, 1992; Vasseur, Kabbert, & Lebert, 1991). These studies showed clearly that the drying submodel depends largely on the conditions of the feed material (moisture content, thermophysical properties etc) and on the operational conditions of the dryer. However, these studies were conducted with single drum dryers which present different operational characteristics than double-drum dryers.

Karapantsios and co-workers (Anastasiades, Thanou, Loulis, Stapatoris, & Karapantsios, 2002; Gavrielidou, Vallous, Karapantsios, & Raphaelides, 2002; Kalogianni, Xinogalos, Karapantsios, & Kostoglou, 2002; Vlachos & Karapantsios, 2000; Vallous, Gavrielidou, Karapantsios, & Kostoglou, 2002) communicated the results of a large experimental campaign (1997–2000) conducted on an industrial scale double-drum dryer for the production of pregelatinized starches. These studies used modern instrumentation and data analysis techniques to investigate the complex phenomena governing the performance of the dryer. The work of Vallous et al. (2002) dealt also with the development of a fluid dynamics submodel. Recently, Kostoglou and Karapantsios (2003) studied the heat transfer submodel of the drum dryer from a mathematical point of view. This work is a step further, aiming to study the drying characteristics of pregelatinized starch thin films in order to identify an appropriate drying submodel for this particular application.

The studies of Vasseur and co-workers and recently the work of Fudym, Carrere-Gee, Lecomte, and Ladevie (2003) (on thin film drying of alumina sludge) concluded that drum drying can be divided in two distinct stages. A short initial period where water is removed by a boiling-type of drying characterized by violent vapour bubble nucleation, growth and detachment, as far as there is free moisture in the material (i.e., down to ~50% moisture content). And a subsequent prolonged conductive type of drying governed by a combination of heat conduction and moisture migration inside the film of the material. It must be noted though that the above differentiation between the two types of drying is only a convention based on their macroscopic characteristics rather than on their underlying physical mechanisms. Daud and Armstrong (1987), also argued about a conductive type of drying of the film spread over the drum surface but claimed that the bulk of moisture loss occurs not in the film zone but in the feeding zone (the gelatinization pool) of the dryer. Apparently, the different type of dryers employed in these studies have played a role in the observations. Most of these studies measured the temperature and heat fluxes of the solid wall and from them determined indirectly the drying rates (with validation chiefly against the moisture of the exit dry product). Only a few have obtained direct loss-in-weight data but then thermal control was cumbersome. In addition, the use of a flat solid plate to simulate the drum's hot surface in very short drying experiments (<10–20 s) arises questions about irregular drying as a result of non-uniformities during the rapid deposition and spreading of the viscous thin film (<1 mm) over the plate.

Apart from drum drying applications, thin film drying of viscous materials has a fundamental significance. A survey of the literature shows that relevant studies are scarce, contrary to the well known problem of thin film drying of water or aqueous solutions films (e.g., Trystram & Vasseur, 1992; Vasseur & Loncin, 1983). Thin films are frequently employed in process equipment e.g., falling film evaporators, as they allow high heat and mass transfer rates (Karapantsios, Kostoglou, & Karabelas, 1995). The transfer increases as the film gets thinner. However, it was early understood that for evaporation from a motionless aqueous film it is not possible to achieve a too low film thickness because the film tears and shrinks forming dry-out patches and as a result the flux reduces (e.g., Nishikawa, Kusada, Yamasaki, & Tanaka, 1967; Zuber & Staub, 1966). The situation with the pregelatinized starch pastes is interesting because the strong adhesion of the film to the heated wall and its progressively increasing viscosity upon drying hinder the film from tearing apart even at a very low film thickness and so fluxes can be particularly high.

Kinetic analysis not only allows estimation of drying rates but also lead to suitable rate expressions characteristic of possible reaction mechanisms. It must be stressed, though, that a satisfactory rate equation does not always provide enough information to establish the reaction mechanism but fortunately this is not a requirement for process equipment design and control. So, the calculated kinetic parameters can be of a great practical value for technological applications since kinetic modeling successfully replaces time- and material-consuming experiments. Drying of gelatinized starch represents a typical situation in terms of kinetic analysis where ideas for heterogeneous reactions approximately apply. This is so because on a microscopic scale the removal of water from the starch solid matrix constitutes a typical heterogeneous process.

The primary purpose of this work is to investigate the kinetics of drying of pregelatinized starches in the form of thin films in an effort to identify a drying rate expression that can be used in drum drying applications. A further objective is to provide insight on the mechanism of water removal from these viscous thin films. First, drying experiments are conducted with a Simultaneous Thermal Analyzer (STA) which combines thermogravimetric (TGA) and differential calorimetry (DSC)

measurements. To the best of our knowledge, this is the first time that synchronous loss-in-weight, heat flow and temperature measurements are recorded in studying starch gels drying. Next, the obtained drying curves are examined if they follow some heterogeneous solid-state kinetic models and also a semi-empirical model from literature that was proposed to hold for single drum drying of another food product.

2. Materials and methods

Commercial maize starch was purchased from Group Amylum S.A., Greece, with an initial moisture content of 13.5%. The total amylose content was $26.0 \pm 0.3\%$, determined by the method of Morrison and Laignelet (1983). The volumetric granule size distribution, as determined in starch suspensions at 20 °C using a Malvern MasterSizer (Malvern Instruments Ltd.) laser diffraction particle size analyzer, was essentially unimodal over the range 6–30 μm with only a very small fraction of particles below 3 μm. The granules mean diameter was 14.95 μm with a standard deviation of 5.8 μm.

Native maize starch was modified according to a thermal scenario that resembles the conditions met by Karapantsios and co-workers in their double-drum dryer. All measurements were conducted with starch/water suspensions of 10% w/w solids content, as this is a concentration that gave good-quality products over a broad range of operational conditions of the double-drum dryer.

2.1. Pasting procedure

About 30 g of native starch/water suspension were added into a 100 ml beaker and placed over a heating plate equipped with a magnetic stirrer. The mixture was heated up while agitated by a magnetic spin bar in order to ensure homogeneity. At around 70 °C, the mixture turned into a viscous paste and from then on stirring was continued manually with a glass rod. Heating and stirring went on until the paste reached a predetermined target temperature. Three target temperatures were employed, 75, 85 and 95 °C, namely, which will be henceforth referred to as *pasting temperatures* of the mixture. These values span the range of temperatures measured inside the pool between the drums of the double-drum dryer, where gelatinization of the feed suspension occurred (Gavrielidou et al., 2002).

The whole pasting procedure lasted 5–8 min, a time similar to the average residence time of the mixture inside the pool of the dryer (Anastasiades et al., 2002; Gavrielidou et al., 2002). The final paste had always a characteristic sticky texture with no discernible clumps or air bubbles. Drying aliquots to constant weight always checked the final solids concentration.

During pasting, some inevitable water evaporation from the processing beaker occurred. This was also happening in the pool of the double-drum dryer where moisture losses were measured to be less than 3% of the total weight (Vallous et al., 2002). In order to match these conditions here, we made preliminary tests with various combinations of beaker sizes versus starch/water quantities and we arrived at the aforementioned values. The employed values provide a comparable V/A (V: heated volume, A: evaporation area) ratio with the pool of the drum dryer.

There is some concern in literature that starch/water suspensions may not have enough time to get fully gelatinized in the pool of drum dryers; this being worse for single drum dryers with auxiliary rollers where the size of the pool is very small (Daud & Armstrong, 1988; Fritze, 1973; Gavrielidou et al., 2002). Therefore, it was decided to perform drying tests not only with samples produced by the aforementioned procedure but also with samples being left for additional 45 or 90 min inside isothermal baths at a temperature equal to their pasting temperature (denoted above). This additional heating period will be henceforth referred to as *pasting duration*. Those samples were hermetically closed inside glass jars to avoid evaporation losses in the bath.

2.2. Drying experiments

Drying of starch/water pastes was studied in a Simultaneous Thermal Analyzer (STA 1500H, Rheometric Scientific), an apparatus where simultaneous thermogravimetric (TGA) and differential calorimetry (DSC) data can be obtained. The apparatus nominal temperature scanning rates were from 0.1 to 60 °C/min, the DSC sensitivity was better than 5 μW and the TGA sensitivity was 0.5 μg.

For every drying run, only a small quantity of the produced paste was used. This quantity was carefully spread over the bottom of aluminum crucibles (open-top cylinders with 4 mm ID and 2 or 4 mm height) to form thin films of different thickness. To allow heat flow only from the bottom of the crucibles, the interior of their side walls was carefully covered with a layer (~0.1 mm) of a low thermal conductivity cement (OB-700, Omega). Films with thickness of 4, 2, 1 and 0.5 mm were tested. For films with thickness 1 and 0.5 mm, crucibles of 2 mm height were used. For the rest, crucibles of 4 mm height were used.

To spread such thin sticky films inside so small receptors required excessive skill. Each measurement was replicated five times. The success in reproducing the films was inversely proportional to their thickness, reflecting the difficulty to handle thinner films. For films of 4 and 2 mm, the variance (=s.d./mean thickness) was better than 0.03 whereas for 1 mm films it was up to 0.06 and for 0.5 mm films up to 0.1. This had a direct effect

on the deviation among drying curves of replicate samples. The overall average variance among repeated drying curves was 0.05.

In drum drying, often thinner films (<0.1 mm) are encountered (e.g., Vallous et al., 2002; Vasseur et al., 1991). Yet, for such thin films, it was not possible to achieve good and uniform contact of the paste with the crucible walls. The significance of using here films thicker than 0.1 mm will be discussed in a subsequent section.

The flow velocity of the cooling agent (Nitrogen) in the test cell of the apparatus was adjusted to only 0.5 m/s in order to suppress the noise in gravimetric measurements and also simulate the low air velocity created by the slow rotation of the drums. This was important in order to avoid convective drying. In fact, the employed gas velocity was not as low as met in double-drum drying where relative air velocities less than 0.1 m/s are often encountered. So, to further diminish convective evaporation losses (especially at temperatures below boiling), the crucibles were covered with a wider crucible, acting as a loose cap, having a small hole in the center. This is a common practice in DSC treatment of samples that are prone to evaporation losses (McNaughton & Mortimer, 1975).

2.3. Thermal scenario

A major concern of this work was to dry the samples using a thermal scenario similar to that observed in the experiments performed in this group with a small industrial double-drum dryer (e.g., Kalogianni et al., 2002; Vallous et al., 2002). It is well known that in drum dryers the temperature of the external drum wall varies in cyclic manner over the period of a revolution (e.g., Trystram & Vasseur, 1992). Thus, in every revolution, the drum surface attains practically the same temperature at each particular angular position. The section of our drums' perimeter where pure drying was taking place (that is, after exiting the pool) is 3/5 of a revolution. In this section, the temperature of the drums surface was initially constant at approximately 105–110 °C and then gradually climbed up to a temperature between 120 and 140 °C, depending on the steam pressure in the drums. To simulate this temperature profile with the STA 1500H proved a difficult task. This is so because the samples should initially be heated from ambient to ~105–110 °C as fast as possible (to suppress preboiling evaporation losses) and after that be very slowly heated to up 120 °C or 140 °C, where they should remain till fully dried. The latter target temperatures will be henceforth symbolically referred to as *drying temperatures*. To achieve a profile as close as possible to the above, the apparatus had to be manipulated so as to overrun the overshoot countermeasures of the thermal regulation system and also account for the thermal inertia of the heating elements. After extensive trials, the most effective programming sequence proved to be a thermalization ramp from ambient to 120 °C (not 105 °C or 110 °C) with a nominal rate of 60 °C/min being followed by a slow ramp of 1 °C/min up to 160 or 180 °C (not 120 or 140 °C). This sequence performed fairly well for 4 and 2 mm samples (in fact, these samples were fully dried already at about 120 or 140 °C so the sequence was interrupted) and had less success for 1 and 0.5 mm samples. This was a result of operating the apparatus under extreme conditions (fast heating ramps along small ΔT and low cooling gas flow rate) where the different heat capacity and latent heat of samples of different thickness (mass) dictated the thermal response of the system.

The parameters that were examined are: (a) film thickness (4, 2, 1 and 0.5 mm), (b) pasting temperature (75, 85 and 95 °C), (c) pasting duration (0, 45 and 90 min) and (d) drying temperature (120 and 140 °C). Due to space limitations, results with 85 °C pasting temperature and 45 min pasting duration will not be presented here, with no real loss of information, whatsoever, since they follow the trends of the other results. The (×-×-×) format in the legends of the plots stands for (pasting temperature–pasting duration–drying temperature).

3. Kinetic analysis

To compare measurements from various experiments for a kinetics investigation and also suppress minor fluctuations of initial sample thickness, it is necessary to introduce a dimensionless degree of loss-in-weight. Thus, by normalizing the instantaneous sample weight, m_t, with respect to some reference value, an index of drying is defined. Taking advantage of the value of m_o before the onset of drying (a maximum) and m_f for a completely dried sample (a minimum), the following degree of loss-in-weight is proposed:

$$\alpha = \frac{m_t - m_f}{m_o - m_f} \tag{1}$$

Completely dried means samples with constant weight at the end of drying. Kinetic studies customary utilize the basic conversion rate equation (e.g., Hill, 1977):

$$\frac{d\alpha}{dt} = k(T) f(\alpha) \tag{2}$$

where $f(\alpha)$ is a conversion dependent function and $k(T)$ is the reaction rate constant.

An integrated expression of Eq. (2) often appears in literature (e.g., Froment & Bischoff, 1979):

$$g(\alpha) = \int_0^{\alpha} \frac{d\alpha}{f(\alpha)} = k(T)t \tag{3}$$

Both $f(\alpha)$ and $g(\alpha)$ are functions representative of theoretical models that must be derived with respect to the mechanism of the reaction.

It is generally accepted that solid–liquid reactions can follow a large variety of kinetic equations. In fact, the apparent occurrence of simple order equations is mainly coincidental (Froment & Bischoff, 1979). Many authors have derived expressions that reflect the nature of various reaction types. These may be conveniently recognised from experimental data using the *Reduced-Time Plot* method of Sharp, Brindley, and Narahari Achar (1966). In this method, all forms of kinetic expressions are written in the form:

$$g(\alpha) = c\frac{t}{t_{0.50}} \tag{4}$$

where c is a constant calculated from the actual form of the kinetic expression, and $t_{0.50}$ is the reaction's half-life (time to 50% conversion).

The selection of the $g(\alpha)$ function is based on the shape of a reduced-time plot which describes best the experimental data. By calculating values of α for nine different kinetic equations and plotting them against $t/t_{0.50}$, Sharp et al. (1966) obtained nine corresponding curves, each one having a characteristic shape. These nine reaction types and their corresponding c values are given in Table 1.

Theoretical predicted fractions, α, versus $t/t_{0.50}$, for the various reactions equations, against experimental data of this study can be seen in Fig. 5b (more about the comparison later). Although the analytical expressions in Table 1 are so different, the respective theoretical curves look quite similar. In fact, data can be classified into three distinct groups. The first group includes the four diffusion equations, the second group includes the moving phase boundary and first order decay equations and the third includes the 2D and 3D random nucleation (Avrami-Erofeev) equations. The proximity between some models in Fig. 5b makes it difficult to identify the correct reaction mechanism. In order to improve the capacity for differentiation within these groups, Rozycki and Maciejewski (1987), proposed to plot α also against $t/t_{0.25}$, and $t/t_{0.75}$, and this idea was employed in the present work. Several authors have successfully used the reduced-time plot method to study the interaction of liquids with a variety of solid materials (e.g., Brown, Dollimore, & Galwey, 1997; Day, Cooney, & Wiles, 1989; Karapantsios, Sakonidou, & Raphaelides, 2002).

Vasseur and co-workers communicated a semi-empirical kinetic model for thin film drying of bakery yeast and a starch-based product (Trystram & Vasseur, 1992; Vasseur et al., 1991). The model was derived from tests on a small thermal regulated plate (100 cm^2) and on a pilot single drum dryer equipped with auxiliary rollers. This model was identified for very thin films (0.05–0.2 mm) that were dried in a very short time (less than 20 s). Therefore, it is considered particularly useful to apply it to the present measurements, keeping in perspective the reservations (Section 1) about probable irregular drying over the hot plate. The obtained form of kinetics is

$$\Phi e(t) = b1 * (T_s(t) - 100)^{b2} * \left(\frac{1}{C}\right)^{b3} * \left(1 - e^{-X(t)/b4}\right)^{b5} \tag{5}$$

where $\Phi e(t)$ is the heat flux utilized for drying in kw/m^2, $T_s(t)$ is the instantaneous temperature of the heating wall in °C, C is the so-called "specific load" in kg dry matter/m^2 (a quantity that does not change during drying), $X(t)$ is the instantaneous moisture content of the film in kg water/kg dry matter and $b1, b2 \ldots b5$ are parameters that must be identified so as to best-fit the experimental data.

The term $(T_s(t) - 100)^{b2}$ in the model accounts for the boiling-type of drying that occurs in early processing times (100 °C: approx. boiling temperate at ambient conditions). The term $(1/C)^{b3}$ describes the inverse proportionality between film thickness and heat flux which is deemed important for such thin films. Finally, the term $(1 - \exp(X(t)/b4))^{b5}$ accommodates what happens during most of the drying period until its end (when the water activity of the material becomes less than one) and pulls gradually the heat flux to zero even if $T_s(t)$ increases.

The heat flux $\Phi e(t)$ is equal to

$$\Phi e(t) = \Phi m(t) * \Delta H_v \tag{6}$$

Table 1
Some common solid-state reaction kinetic equations

Reaction type, $g(\alpha)$	c-Value	Rate-controlling process
$D_1(\alpha) = \alpha^2$	0.2500	Diffusion, 1D
$D_2(\alpha) = (1-\alpha)\ln(1-\alpha) + \alpha$	0.1534	Diffusion, 2D
$D_3(\alpha) = [1-(1-\alpha)^{1/2}]^2$	0.0426	Diffusion, 3D (spherical symmetry)
$D_4(\alpha) = (1-2\alpha/3) - (1-\alpha)^{2/3}$	0.0367	Diffusion, 3D (contracting sphere model)
$R_2(\alpha) = [1-(1-\alpha)^{1/2}]$	0.2929	Moving phase boundary, 2D
$R_3(\alpha) = [1-(1-\alpha)^{1/3}]$	0.2063	Moving phase boundary, 3D
$F_1(\alpha) = \ln(1-\alpha)$	−0.6931	Random nucleation, first order decay law
$A_2(\alpha) = [-\ln(1-\alpha)]^{1/2}$	0.8326	Random nucleation, two dimensional
$A_3(\alpha) = [-\ln(1-\alpha)]^{1/3}$	0.8850	Random nucleation, three dimensional

where ΔH_v is the latent heat of water evaporation in kJ/kg and $\Phi m(t)$ is the moisture (removal) mass flux in kg/m^2. For the mass flux it holds

$$\Phi m(t) = \frac{\mathrm{d}m(t)}{\mathrm{d}t} = C * \frac{\mathrm{d}X(t)}{\mathrm{d}t} \tag{7}$$

where $m(t)$ is the instantaneous weight of the sample. To fit the experimental data to Eq. (5) a non-linear numerical regression is performed by the Levenberg–Marquardt method which gradually shifts the search for the minimum χ^2 from steepest descent to quadratic minimization (Gauss–Newton). For all the regressions, the latent heat value for water was kept constant at 2257 kJ/kg.

4. Results and discussion

4.1. Temperature profiles

Fig. 1a–d, present the temperature profiles obtained for the various samples and thermal treatments. These temperatures are actually measured at the crucible holding the samples and not the samples themselves and so one may see them with reservation. However, for standard thermal analysis equipment such as STA 1500H and except for extreme operating conditions there will be a very small difference and time lag between crucible and sample. The curves in Fig. 1a–d bear several features in common. The initial gradual rise till ~40 °C is followed by a steep ascent till ~110 °C. Unfortunately, this initial thermalization of the sample represents only about half of the programmed maximum heating rate of the apparatus (60 °C/min).

From this point on, the temperature tends progressively to level off towards 120 °C or 140 °C, this behavior being more successful for 120 °C and thicker films. In fact, for the thinner films, the material dries so quickly (on a relative basis) that the temperature climbs constantly up. It must be noted that for the 0.5 mm samples, the temperature profiles obtained for the two drying temperatures are hardly distinguishable, as the apparatus failed to comply sufficiently with the programmed thermal sequence. Yet, the differential calorimetry and gravimetric analysis (see below) was able to discern minor differences between them. Overall, the same programmed thermal sequences produced appreciably different profiles for samples of different thickness. One should keep in mind these discrepancies for the analysis below.

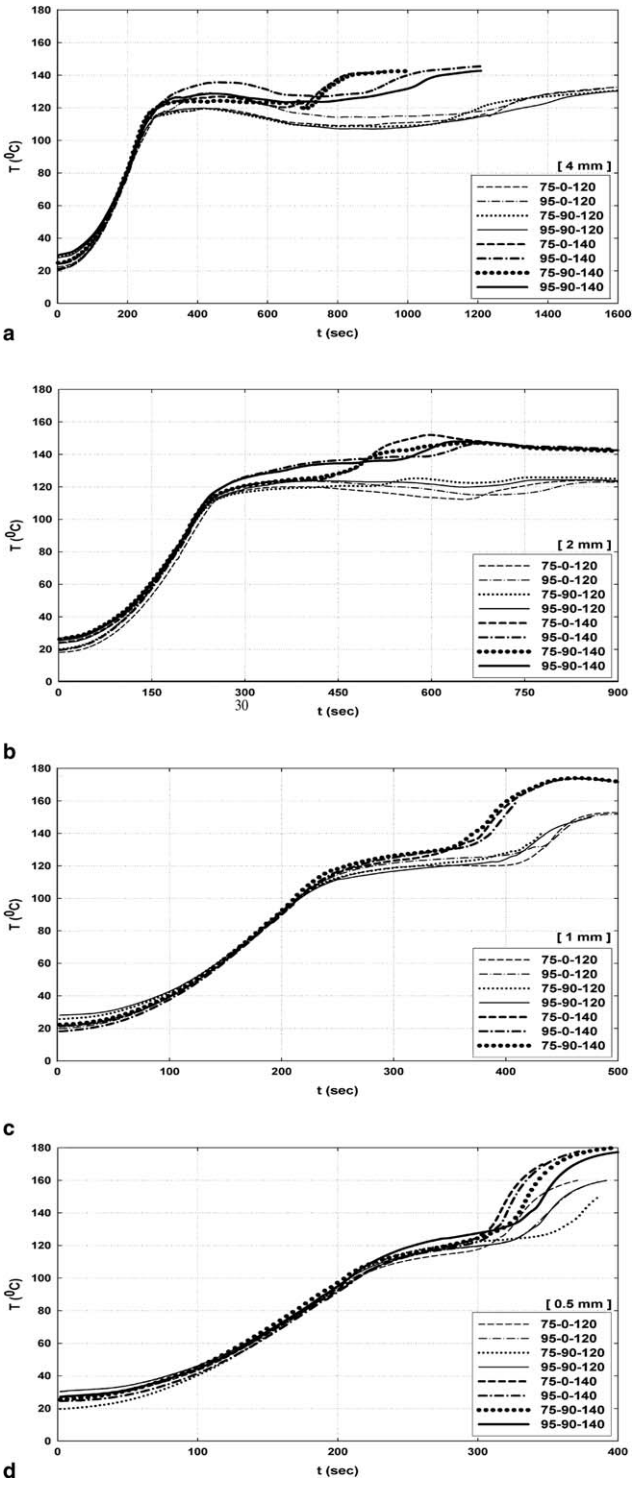

Fig. 1. Temperature profiles for all the examined conditions and for films of varying thickness: (a) 4 mm, (b) 2 mm, (c) 1 mm and (d) 0.5 mm.

4.2. Drying curves

Fig. 2a–d, display curves of degree of loss-in-weight, α, versus drying time. If one combines Figs. 1 and 2, interesting observations can be made. In all curves, there are only limited evaporation losses below 100 °C due to the employed fast initial thermalization period and the presence of the protective loose cap over the crucible. Such losses are more prominent, on a percentage basis, with thinner films. Right above 100 °C, the drying

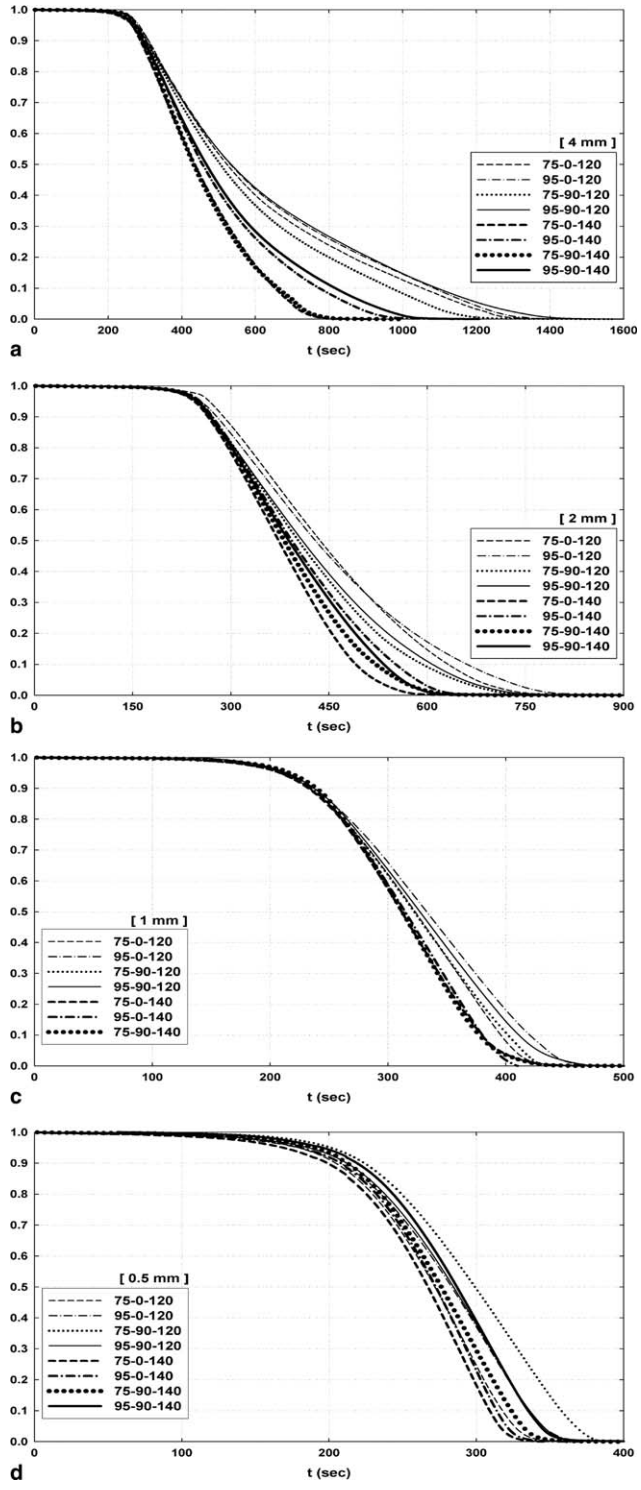

Fig. 2. Degree of loss-in-weight, α, versus time for all the examined conditions and for films of varying thickness: (a) 4 mm, (b) 2 mm, (c) 1 mm and (d) 0.5 mm.

curves turn into a progressively steeper descent until they attain a maximum slope (max drying rate). Near the end of drying, the curves turn gradually into a gentle decay towards zero (final dry mass).

In the curves of Fig. 2, the overall drying rate, coarsely inferred as the reciprocal of the elapsed time to complete the process, appears to depend strongly on film thickness and much less on the other examined variables. The thicker the film, the lower the drying rate. Furthermore, for the 4 mm films there is a clear dependence of the drying rate on drying temperature and a less pronounced dependence on pasting temperature (more visible at 140 °C drying temperature). For a higher drying temperature and a lower pasting temperature drying occurs faster. The latter has most likely to do with the different degree of solubilization of starch components at 75 and 95 °C, respectively. It is chiefly amylose that solubilizes at 75 °C whereas both amylose and amylopectin solubilize at 95 °C and so the consistency of the solid matrix is different at the two temperatures (e.g., Anastasiades et al., 2002; Doublier, 1981). On the other hand, some subtle dependence of the drying rate on the pasting duration is within the statistical error of the determination and so is not reliable. Going down to thinner films, the dependencies observed in the 4 mm films progressively fades out and ultimately for 0.5 mm films there is no clear dependence on any variable. The latter is not surprising if one considers the similar temperature profiles obtained for all the runs with 0.5 mm films (Fig. 1d). A possible reason for this may be the relatively large variance in the produced thickness of such thin films.

Fig. 3a–d present the normalized drying rate, $d\alpha(t)/dt$, versus time for all the runs of Fig. 2. The data are not as smooth as in Fig. 2 due to the derivatization that accentuates any noise in the original data. As expected, the higher moisture removal rates occur for the thinner films. In line with Figs. 1 and 2 d, for the 0.5 mm films the curves of the two drying temperatures overlap to some extent. The situation improves with the thicker films where one can distinguish the 120 °C from the 140 °C curves.

What is perhaps of greater significance is the shape of the curves for the various films. For 0.5 mm films, the curves are skewed (asymmetric) to the left but as the thickness increases the skewness shifts to the right. For all films, there is virtually no constant drying rate period before the falling rate period.

The duration of the falling rate period varies proportionally with the film thickness of the samples. This may be attributed to the different increase in the viscosity of the samples (as their dry matter accumulates) which hampers the bubble-induced convection and resists heat transfer. Cross-inspection of Figs. 2 and 3 shows that for films less than 1 mm the falling rate periods of the curves start at below 50% w/w water content. However, for 2 and 4 mm films the falling rate period starts at much higher moisture contents. If one intuitively considers the falling rate period to represent a conductive type of drying (as explained in Eq. (5)) then all the above indicate a direct effect of the thickness of the film to the

observed type of drying. Thinner films dry so fast that a falling rate period is encountered only at the end of drying; most of the moisture is removed by boiling. As the film thickness increases (and drying occurs slower), boiling drying recedes in favor of conductive drying.

4.3. Heat flow curves

To shed some light into the above arguments, Fig. 4a–d display the instantaneous heat flow time records obtained for all films. In all curves, there is a val-

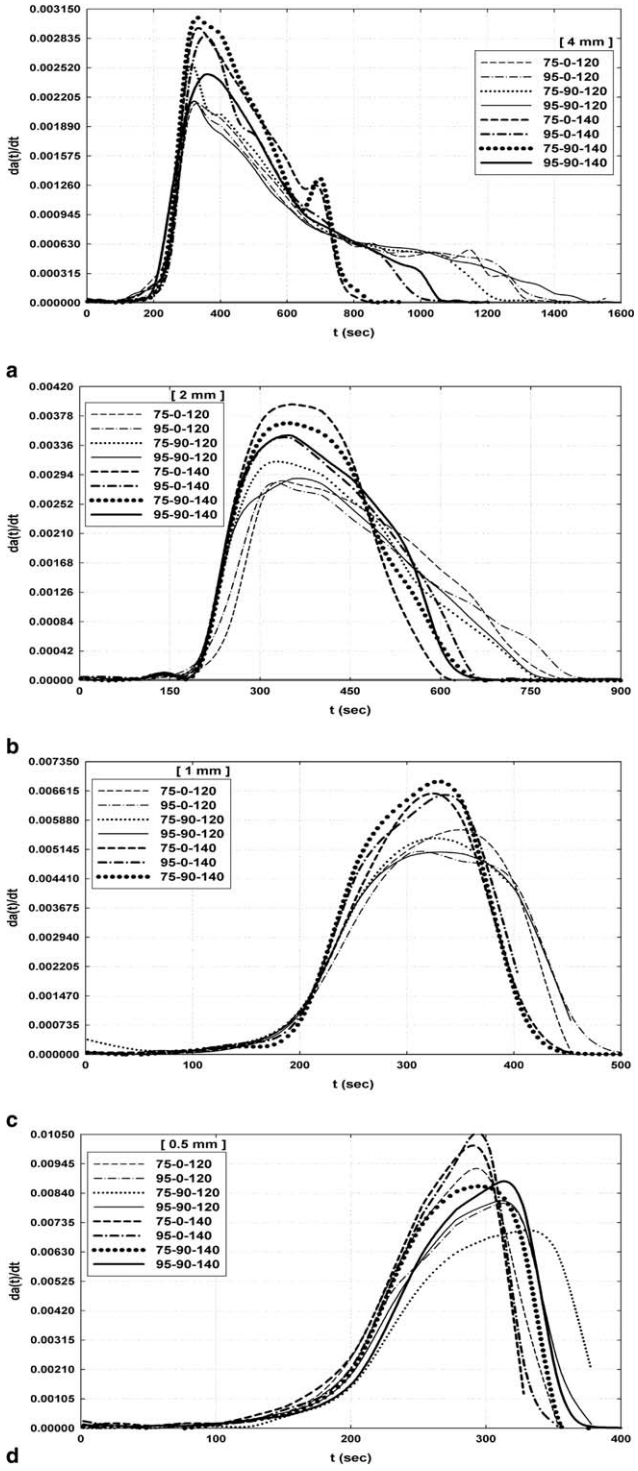

Fig. 3. Normalized drying rate, $d\alpha(t)/dt$, versus time for all the examined conditions and for films of varying thickness: (a) 4 mm, (b) 2 mm, (c) 1 mm and (d) 0.5 mm.

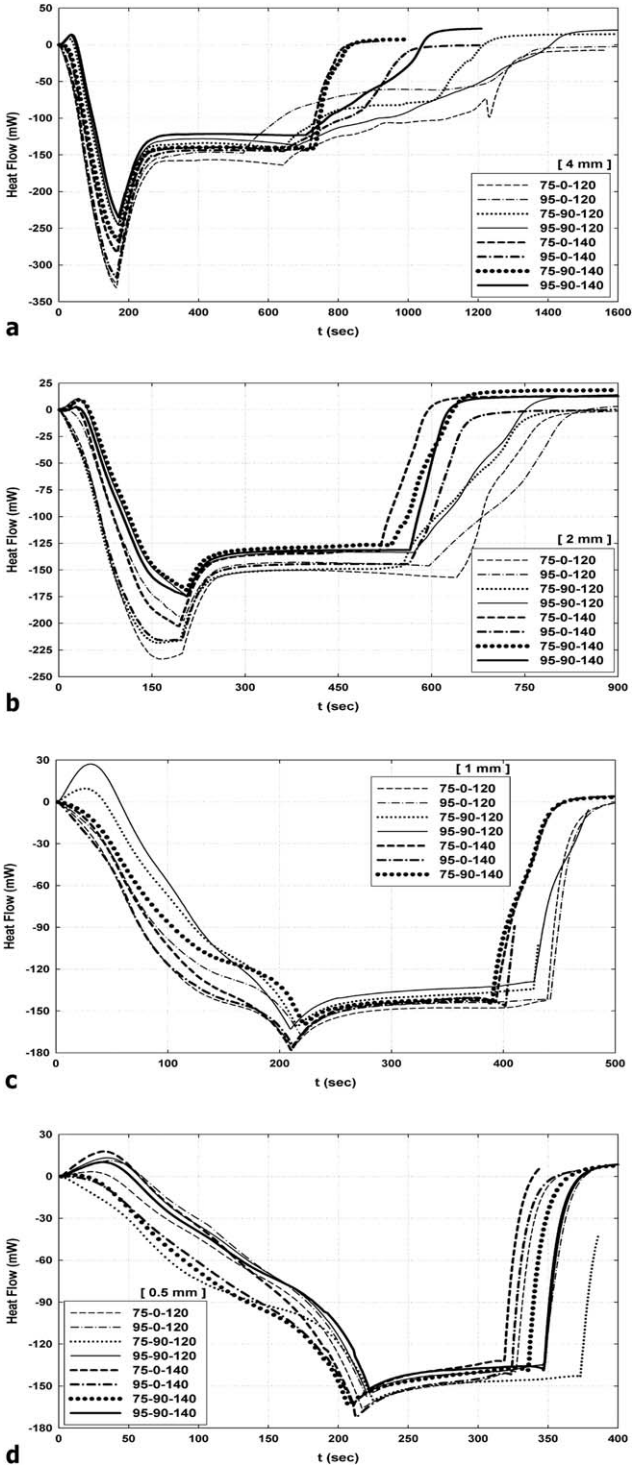

Fig. 4. Heat flow versus time for all the examined conditions and for films of varying thickness: (a) 4 mm, (b) 2 mm, (c) 1 mm and (d) 0.5 mm.

ley which represents the maximum (negative for endothermic) heat supply to the sample. The valley is deeper for the thicker films (4 and 2 mm) and reflects the increased heat capacity, latent heat and thermal inertia of these samples compared to the 1 and 0.5 mm films. After passing the valley, the heat flow curves rapidly climb up and level-off to an approximately constant value at ~140–150 mW, regardless the film thickness. This constant heat flow rate most likely corresponds to isobaric boiling which (at a roughly constant surface overheat, Fig. 1) is dictated by the surface area for evaporation (cross-section of the crucible) and not the sample mass. The calculated corresponding heat flux value is of the order of 10^4 W/m^2 which is a reasonable value for nucleate boiling of a viscous solution (McCabe, Smith, & Harriot, 2001; Vasseur & Loncin, 1983).

Interesting observations can be made when comparing Fig. 4 with Figs. 1–3. One should keep in perspective that a small time lag may exist between gravimetric and heat flow measurements but this is not expected to be substantial. The constant heat flow period stops at a film moisture content that varies among the different runs. For the 4 mm film, this characteristic moisture content depends strongly on drying temperature and to a lesser extent on pasting temperature. The higher the drying temperature and the lower the pasting temperature, the lower the moisture content where heat flow changes. This is rather normal and reflects the decisive role of both the surface temperature and material texture in drying. The situation is less pronounced but still visible in the 2 mm films. Yet, it fades out for the 1 and 0.5 mm films where the constant heat flow period spans almost the entire course of drying down to less than ~3% residual moisture. Apparently, film thickness affects seriously the features of drying, producing disproportionally larger drying rates for films thinner than 1 mm, (Fig. 3). The constant heat flow periods covering part of the falling rate periods shown in Fig. 3 may imply that the removal of vapor (produced by boiling) from the sample is gradually hindered by mass transfer inside the viscous film. So, for the examined starch films it appears that when the thickness becomes less than 1 mm the conductive drying contribution recedes in favor of a boiling-type of drying.

4.4. Kinetic results

Next, the possibility that the drying data follow a common heterogeneous reaction type (Table 1) is examined. Of course, this has a meaning only for the conductive part of a drying curve and therefore this analysis is performed only with 2 and 4 mm films which present an appreciable conductive drying contribution. A requirement for the reduced-time plot method is that the kinetic data are obtained under isothermal conditions. So, from the data for 4 and 2 mm films only the runs that remained at a constant temperature (±3 °C) for an appreciable period of time are selected for kinetic analysis. To avoid the ambiguity of the initial non-isothermal drying period (from 100 to 120 °C), a new time series of degree of loss-in-weight, α', is calculated assuming that the reaction (drying) begins when the temperature reaches steady conditions. It must be stressed that even at 120 °C boiling may still exist inasmuch as there is free water in the samples.

In Fig. 5a–c, data for one film (4 mm, 75-0-140) are compared with the nine kinetic equations of Table 1.

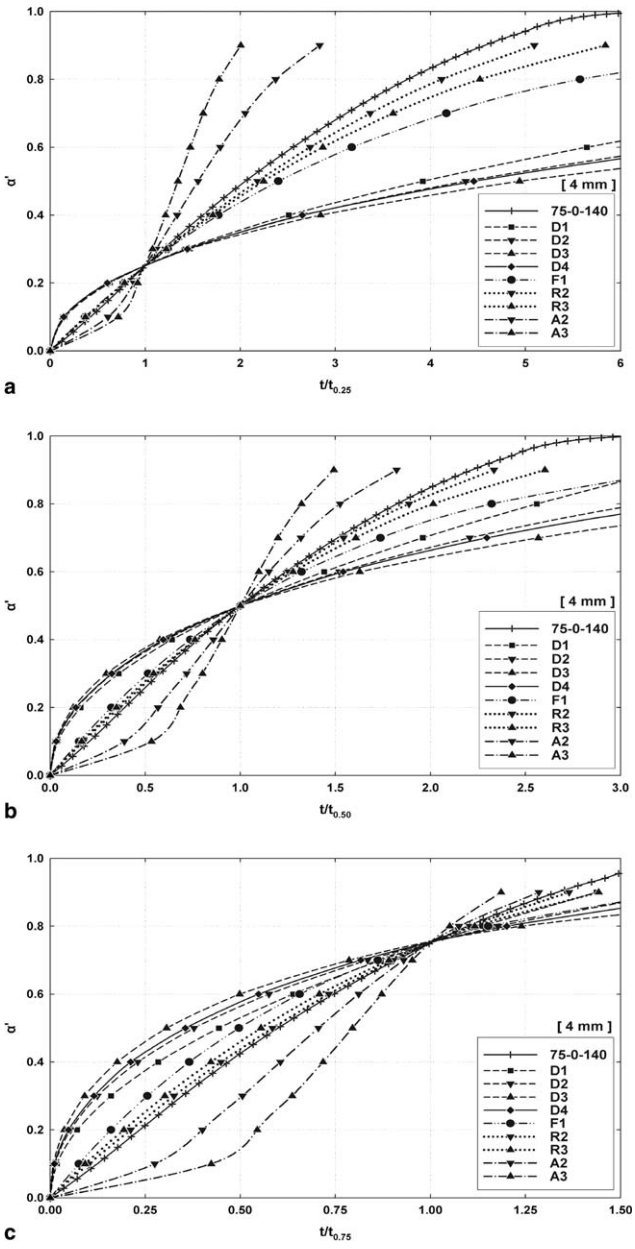

Fig. 5. Reduced-time plot of degree of loss-in-weight, α', versus (a) $t/t_{0.25}$, (b) $t/t_{0.50}$ and (c) $t/t_{0.75}$ along with theoretical curves calculated for various solid-state reaction equations. The plotted data are quasi-isothermal measurements from the run with a 4 mm film thickness, 75 °C pasting temperature, 0 min pasting duration and 140 °C drying temperature. Symbols explained in Table 1.

As can been seen, in all plots the drying data fall very close to the $R_2(\alpha)$ curve. The theoretical basis on which the $R_2(\alpha)$ model is based assumes a reaction (drying) mechanism in which the rate determining step is the movement of a flat reaction zone (e.g., water front) inside the sample up to its free surface. The mechanism of water removal from the starch film is therefore easy to visualize.

All the analyzed runs, along with the $T_{\alpha'=0}$ (onset temperature of isothermal drying) and the results of the reduced-time plot method are presented in Table 2. As can be seen, for the 2 mm films, the $R_2(\alpha)$ model describes closely the measurements. However, for the 4 mm films, best-fit with the experimental values is achieved not only with the $R_2(\alpha)$ but also with the $R_3(\alpha)$ and $F_1(\alpha)$ models. The latter two models represent volumetric (3D) mechanisms which demonstrate the significant role of the volume of sample as compared to its surface area in drying (Hill, 1977). So, for thicker films a shift in the dominant mechanism of conductive drying is probable. Evidently, measurements over a broad range of conditions are required before definitive statements can be made.

Fig. 6 displays the regression analysis to fit data from four runs altogether (75 °C–0 min–140 °C and for 0.5, 1, 2, 4 mm films) to Vasseur et al. model predictions (Eq. (5)). The calculated heat flow rates have values close to those reported by Vasseur et al. (1991) and Abchir et al. (1988) in drying thin films of viscous beaker's yeast.

For clarity in the presentation, the data of the four films are shifted in the time domain so as not to overlap. Fig. 6a shows the fitting to the full equation (5) whereas Fig. 6b shows the fitting to Eq. (5) without the term $(1/C)^{b3}$. The effect of the specific load (film thickness) term appears not so important for describing the heat flux in the 2 and 4 mm films but important for the thinner films. However, this is only due to the fact that the exponential (conductive) term of the model is dominant

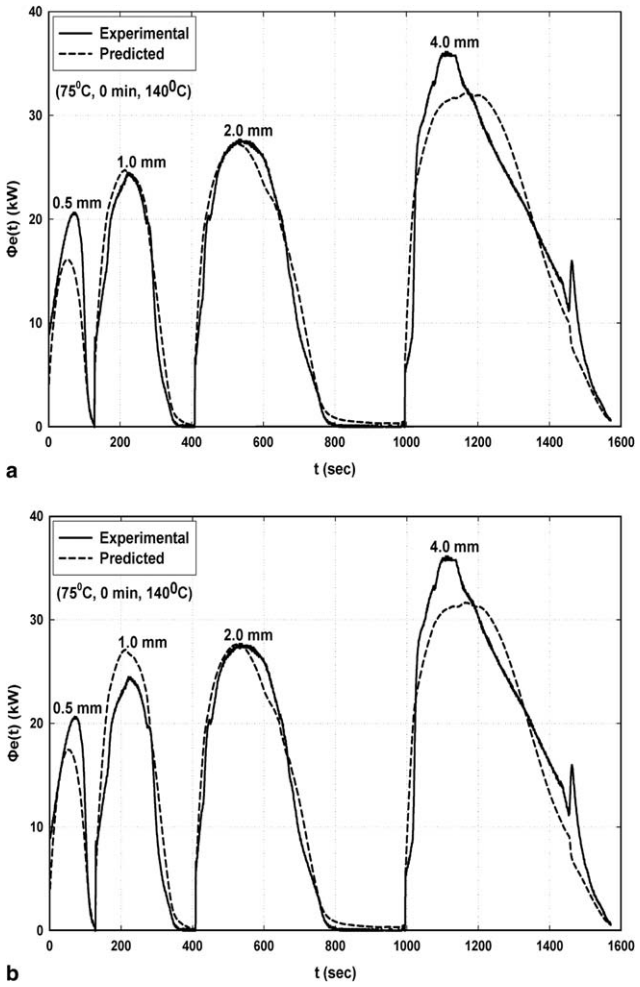

Fig. 6. Regression results based on Eq. (5) against experimental data for films with thickness 0.5, 1, 2 and 4 mm film and for 75 °C pasting temperature, 0 min pasting duration and 140 °C drying temperature: (a) with the specific load term and (b) without the specific load term (case #37 in Table 3).

Table 2
Results of the reduced-time plot method for all the quasi-isothermal runs

Thickness (mm)	$T_{pasting}$ (°C)	$t_{pasting}$ (min)	T_{drying} (°C)	$T_{\alpha'=0}$ (°C)	Best-fit model
4	75	0	120	116	$F_1(\alpha)$
≫	≫	≫	140	120	$R_2(\alpha)$
≫	≫	90	120	116	$F_1(\alpha)$ and $R_3(\alpha)$
≫	≫	≫	140	118	$R_2(\alpha)$
≫	95	0	120	119	$F_1(\alpha)$
≫	≫	≫	140	123	$R_3(\alpha)$
≫	≫	90	120	117	$F_1(\alpha)$
≫	≫	≫	140	120	$R_3(\alpha)$
2	75	0	120	118	$R_2(\alpha)$
≫	≫	90	≫	118	$R_2(\alpha)$
≫	95	0	≫	117	$R_2(\alpha)$
≫	≫	90	≫	118	$R_2(\alpha)$

for the thicker films where boiling occurs only at the beginning of drying and before the viscous paste turns into a firm gel. Therefore, when later the product becomes dry enough, boiling ceases and the heat flux decreases exponentially in spite of the rising temperature of the gel. In conclusion, the composite semi-empirical model of Vasseur et al. seems to predict adequately the heat flow rates involved in drying the starch films of this study.

Table 3 presents the results of the statistical analysis to fit Eq. (5) to all our data, including the specific load term. The goodness of the fitting for each individual run (set of conditions) was very good, ($R^2 = 0.940$–0.997). Interestingly, when we tried to fit the model collectively to all our data (last line in Table 3) then the goodness of the fitting was not dramatically reduced ($R^2 = 0.919$). Therefore, in view of the different conditions between the experiments of Vasseur et al. and

Table 3
Results of the regression analysis to fit Eq. (5) to experimental data

#	$T_{pasting}$ (°C)	$t_{pasting}$ (min)	T_{drying} (°C)	Thickness (mm)	$b1$	$b2$	$b3$	$b4$	$b5$	χ^2	R^2
2	75	0	120	0.5	3.44	0.592	–	0.462	1.126	27.4	0.995
3	≫	≫	≫	1	1.963	0.749	–	0.248	1.508	53.6	0.997
4	≫	≫	≫	2	0.375	1.355	–	0.299	1.691	427.8	0.991
5	≫	≫	≫	4	1.223	1.078	–	3.671	0.628	4966	0.949
6	75	0	140	0.5	3.823	0.555	–	0.389	1.157	35.1	0.993
7	≫	≫	≫	1	1.439	0.891	–	1.055	1.275	245	0.990
8	≫	≫	≫	2	1.017	1.062	–	1.186	1.306	307.9	0.995
9	≫	≫	≫	4	1.539	1.046	–	7.784	0.480	4058?	0.938
10	75	90	120	0.5	1.405	0.808	–	0.539	0.750	34.8	0.987
11	≫	≫	≫	1	1.574	0.856	–	3.174	0.391	71.8	0.969
12	≫	≫	≫	2	0.965	1.158	–	2.604	0.845	509.2	0.991
13	≫	≫	≫	4	2.395	0.879	–	3.811	0.591	3775?	0.966
14	75	90	140	0.5	2.457	0.722	–	0.581	1.036	96.5	0.992
15	≫	≫	≫	1	0.543	1.154	–	0.859	1.565	205.3	0.993
16	≫	≫	≫	2	0.567	1.305	–	2.347	1.167	745.7	0.991
17	≫	≫	≫	4	0.143	1.827	–	5.507	0.701	3211?	0.976
18	95	0	120	0.5	2.565	0.644	–	0.66	1.195	32.7	0.994
19	≫	≫	≫	1	–	–	–	–	–	–	–
20	≫	≫	≫	2	1.126	0.944	–	2.295	0.554	524.7	0.987
21	≫	≫	≫	4	–	–	–	–	–	–	–
22	95	0	140	0.5	3.029	0.647	–	0.824	1.291	44.1	0.995
23	≫	≫	≫	1	1.747	0.78	–	0.729	0.688	87.2	0.983
24	≫	≫	≫	2	–	–	–	–	–	–	–
25	≫	≫	≫	4	–	–	–	–	–	–	–
26	95	90	120	0.5	1.788	0.769	–	0.446	1.130	45.3	0.993
27	≫	≫	≫	1	2.852	0.662	–	0.921	1.07	142.1	0.983
28	≫	≫	≫	2	1.896	0.903	–	6.832	0.566	347.8	0.992
29	≫	≫	≫	4	5.15	0.665	–	8.52	0.593	1901	0.977
30	95	90	140	0.5	1.212	0.852	–	0.476	1.197	75.2	0.993
31	≫	≫	≫	1	–	–	–	–	–	–	–
32	≫	≫	≫	2	1.203	0.937	–	2.739	0.684	1040.8	0.985
33	≫	≫	≫	4	2.776	1.067	–	31.8	0.653	1051.1	0.991
34	95	90	140	*	4.24	0.825	0.343	13.8	0.61	14302	0.940
35	95	0	140	*	–	–	–	–	–	–	–
36	75	90	140	*	1.146	1.141	0.215	2.888	0.882	14267	0.949
37	75	0	140	*	2.599	0.807	0.138	1.771	0.824	10267	0.949
38	75	90	120	*	2.151	0.933	0.246	3.528	0.616	7223	0.960
39	95	90	120	*	3.457	0.695	0.05	3.943	0.608	7339	0.950
40	75	0	120	*	0.557	1.300	0.187	0.749	1.002	11959	0.931
41	*	*	120	*	2.357	0.834	0.144	2.779	0.627	35398	0.929
42	*	*	140	*	2.416	0.842	0.046	3.886	0.692	62757	0.912
43	*	*	*	*	2.831	0.785	0.101	3.411	0.655	101615	0.919

For the runs where all film thicknesses are included in the analysis, the specific load parameter ($b3$) is calculated. The symbol * in the table is a wild card representing all values of the particular parameter.

the present ones, the overall performance of the model is considered acceptable. The physical significance behind this success is that thin film drying of viscous materials, that do not tear and give dry patches upon drying, can be adequately described by a boiling mechanism combined with an exponential decay mechanism to accommodate the final stages of drying.

The success of the $R_2(\alpha)$, $R_3(\alpha)$ and $F_1(\alpha)$ models does not oppose the success of the Vasseur et al. model which includes an exponential term to accommodate a conductive drying contribution. Besides, the predictions of $R_2(\alpha)$ and $R_3(\alpha)$ are very close to the exponential decay model $F_1(\alpha)$.

5. Conclusions

The purpose of the present work was to examine the kinetic characteristics of drying gelatinized starch in the form of thin films. A Simultaneous Thermal Analyzer (STA) which combines in one instrument a thermogravimetric analyzer (TGA) and a differential scanning calorimetry (DSC) was used to achieve this goal. Among the examined input variables (film thickness, drying temperature, pasting temperature and pasting duration), the thickness of the film influenced mostly the drying rates, being followed afar by the drying temperature. The effect of the pasting temperature was much smaller and

was only witnessed in the thicker films. No statistically significant effect of pasting duration was noticed. Comparisons of heat flow and drying rate data indicate that thin film drying of pregelatinized starch over a hot surface in the absence of forced airflow follows both a boiling-type and a conductive type of drying. Boiling occurs chiefly at the beginning of drying when the starch/water viscous paste has not yet fully transformed to a solid-like gel. For the thinner films of this work (0.5 and 1 mm), boiling appears to prevail over most of the drying period. For the thicker films (2 and 4 mm), conductive drying comes gradually into play at the late stages of drying and there is evidence that co-exists with boiling for some time. A heterogeneous reactions kinetic analysis performed for the 2 and 4 mm films showed that the obtained drying curves are described adequately well by a moving phase boundary mechanism (2D or 3D) or a simple first order exponential law. The latter mechanism is in accord with the semi-empirical model proposed by Vasseur et al. (1991) which by incorporating a boiling and a conductive (exponential) term describes closely all the data of the present work, regardless film thickness.

Acknowledgements

I am grateful to Mr. Demetrios Papastergiou for operating the STA 1500H apparatus in the Lab of Transport Processes & Process Equipment at the Department of Mechanical and Industrial Engineering of the University of Thessaly, Greece.

References

Abchir, R., Vasseur, J., & Trystram, G. (1988). Modelisation and simulation of drum drying. In *Proceedings of the sixth international drying symposium, Versailles, France.* (pp. OP.435–OP.439).

Anastasiades, A., Thanou, S., Loulis, D., Stapatoris, A., & Karapantsios, T. D. (2002). Rheological and physical characterization of pregelatinized maize starches. *Journal of Food Engineering, 52*, 57–66.

Brown, M. E., Dollimore, D., & Galwey, A. K. (1997). Thermochemistry of decomposition of manganese (II) oxalate dihydrate. *Thermochimica Acta, 21*(1), 103–110.

Colonna, P., Buleo, A., & Mercier, C. (1987). Physically modified starches. In T. Galliard (Ed.), *Starch: Properties and potential. Critical reports on applied chemistry* (vol. 13, pp. 79–114). New York: John Wiley.

Daud, W. R. b. W., & Armstrong, W. D. (1987). Pilot plant study of the drum dryer. In A. S. Mujumdar (Ed.), *Drying'87* (pp. 101–108). New York: Hemisphere Publishing Co.

Daud, W. R. b. W., & Armstrong, W. D. (1988). Conductive drying characteristics of gelatinized rice starch. *Drying Technology, 6*(4), 655–674.

Day, M., Cooney, J. D., & Wiles, D. M. (1989). A kinetic study of the thermal decomposition of poly(aryl-ether-ether-ketone) PEEK in nitrogen. *Polymer Engineering and Science, 29*, 19–22.

Doublier, J. L. (1981). Rheological studies on starch-flow behavior of wheat starch pastes. *Starch/Starke, 33*, 415–420.

Fritze, H. (1973). Dry gelatinized produced on different types of drum dryers. *Industrial Engineering, Chemistry, Process Design and Development, 12*(2), 142–148.

Froment, G. F., & Bischoff, K. B. (1979). *Chemical reactor analysis and design* (pp. 3–47, 76–130, 141–149). New York: John Wiley and Sons.

Fudym, O., Carrere-Gee, C., Lecomte, D., & Ladevie, B. (2003). Drying kinetics and heat flux in thin-layer conductive drying. *International Communications in Heat and Mass Transfer, 30*(3), 333–347.

Hill, C. G. (1977). *An introduction to chemical engineering kinetics and reactor design* (pp. 24–166). New York: John Wiley and Sons.

Hodge, S., & Osman, M. (1976). Carbohydrates. In O. R. Fennema (Ed.), *Food chemistry, Principles of food science part 1* (pp. 102–114). NY: Marcel Dekker Inc.

Gavrielidou, M. A., Vallous, N. A., Karapantsios, T. D., & Raphaelides, S. N. (2002). Heat transport to a starch slurry gelatinizing between the drums of a double drum dryer. *Journal of Food Engineering, 54*(1), 45–58.

Kalogianni, E., Xinogalos, V., Karapantsios, T. D., & Kostoglou, M. (2002). Effect of feed concentration on the production of pregelatinized starch in a double drum dryer. *Lebensmittel-Wissenschaft & Technologie, 35*(8), 703–714.

Karapantsios, T. D., Kostoglou, M., & Karabelas, A. J. (1995). Local condensation rates of steam/air mixtures in direct contact with a falling liquid film. *International Journal of Heat and Mass Transfer, 38*(5), 779–794.

Karapantsios, T. D., Sakonidou, E. P., & Raphaelides, S. N. (2002). Water dispersion kinetics during starch gelatinization. *Carbohydrate Polymers, 49*(4), 479–490.

Kostoglou, M., & Karapantsios, T. D. (2003). On the thermal inertia of the wall of a drum dryer under a cyclic steady state operation. *Journal of Food Engineering, 60*, 453–462.

McCabe, W. L., Smith, J. C., & Harriot, P. (2001). *Unit operations of Chemical Engineers* (6th ed.). NY: McGraw-Hill.

McNaughton, J. L., & Mortimer, C. T. (1975). Differential scanning calorimetry. *IRS: Physical Chemistry series* (vol. 10, pp. 37–41). London: Butterworths.

Moore, J. G. (1995). Drum dryers. In A. S. Mujumdar (Ed.). *Handbook of industrial drying* (vol. 1, 2nd ed., pp. 249–262). Marcel Dekker Inc.

Morrison, W. R., & Laignelet, B. (1983). An improved colorimetric procedure for determining apparent and total amylose in cereal and other starches. *Journal of Cereal Science, 1*, 9–20.

Nishikawa, K. H., Kusada, K., Yamasaki, K., & Tanaka, K. (1967). Nucleate boiling at low liquid levels. *Bulletin of the JSME, 10*, 328–338.

Rozycki, C., & Maciejewski, M. (1987). Method of the selection of the $g(a)$ function based on the reduced-time plot. *Thermochimica Acta, 122*, 339–354.

Sharp, J. H., Brindley, G. W., & Narahari Achar, B. N. (1966). Numerical study for some commonly used solid state reaction equations. *Journal of the American Ceramic Society, 49*, 379–382.

Trystram, G., Meot, J. M., Vasseur, J., Abchir, F., & Couvrat-Desvergnes, B. (1988). Dynamic modeling of a drum dryer for food products. In *Proceedings of the sixth international drying symposium, Versailles, France* (pp. PA.13–PA.18).

Trystram, G., & Vasseur, J. (1992). The modeling and simulation of a drum dryer. *International Chemical Engineering, 32*(4), 689–705.

Vallous, N. A, Gavrielidou, M. A., Karapantsios, T. D., & Kostoglou, M. (2002). Performance of a double drum dryer for producing pregelatinized maize starches. *Journal of Food Engineering, 51*, 171–183.

Vasseur, J., Kabbert, R., & Lebert, A. (1991). Kinetics of drying in drum drying. In A. S. Mujumdar & I. Filkova (Eds.), *Drying'91* (pp. 292–300). Amsterdam: Elsevier Applied Science Publishers.

Vasseur, J., & Loncin, M. (1983). High heat transfer coefficient in thin film drying: Application to drum drying. In B. M. McKenna (Ed.), *Proceedings of 3rd international congress, Dublin, Ireland. Engineering and food, vol. 1: Engineering sciences in the food industry* (pp. 217–225). Barking, Essex: Elsevier Applied Science.

Vlachos, N. A., & Karapantsios, T. D. (2000). Water content measurement of thin sheet starch products using a conductance technique. *Journal of Food Engineering, 46*(2), 91–98.

Zuber, N., & Staub, F. W. (1966). Stability of dry patches forming in liquid films flowing over heated surfaces. *International Journal of Heat and Mass Transfer, 9*, 897–905.